

## HORIZONTAL - LOADING TEST OF STEEL BAR-TIMBER COMPOSITE COLUMNS FOR LOW- RISE BUILDING

**Yuuto Shimoirisa<sup>1</sup>, Takahiro Iju<sup>2</sup>, Takao Ohta<sup>3</sup>, Kazuya Mori<sup>4</sup>, Shinichi Shioya<sup>5</sup>**

**ABSTRACT:** In light of the current climate crisis, there has been much recent interest in using timber structural members in large buildings, and moreover, in severe earthquake prone, such as Japan, they are more desired on the grounds of light weight of timber members. We are developing a frame system formed by timber members reinforced by deformed steel bars (i.e. rebars) using epoxy resin adhesive. The column could produce, in mechanical properties, better performance than those of reinforced concrete structure (RC). This paper reports horizontal-loading experiment of its column specimens, its results. The specimens were modelled for three-storey buildings, i.e., low-rise buildings. Performance of the specimens indicated to be better than that of RC columns with the same size except difference in material between wood and concrete.

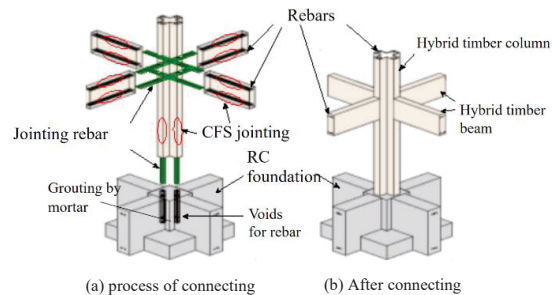
**KEYWORDS:** Composite timber, Column, Deformed steel bar, Moment-resisting connection, Re-centering

## 1 INTRODUCTION




In light of the current climate crisis, there has been much recent interest in using timber structural members in large buildings, as timber is a renewable natural resource. Cross-laminated timber (CLT) is a typical timber element, however, CLT structural system very often restricts building planning, owing to CLT being a plate member. The demand for a timber structural system of slender beams and columns is high.

S. Shioya has proposed a structural system for building construction, adopting Hybrid Glulam Timber members using Steel bars (HGTSB, nicknamed as “Samurai” in Japan), has developed the structural design methodology, and has constructed the first prototype building, a two-way frame structure using the structural system [1,2].

We are now developing more refined and more commercial competitive structural system for buildings adopting HGTSB and its structural design methodology. This paper reports an experimental loading test of columns for low-rise buildings with three storeys or less.



*Figure 1: Beams-column-footing connection*

Cross-Sectional Shape			
Rebar	16-D25	12-D25	12-D25
Rebar $\phi$	630x630	630x630	630x630

**Figure 2: Representative cross-section of column**

S. Shiya has already developed a technique for rigid connection of rebars inside the composite timber, using carbon fiber plastic sleeve (CFS) and epoxy resin adhesive with works similarly to work process of the glued-in-rod, and reported performance of the column adopted the technique as shown in Figure 1 [2,4].

### 3 CROSS-SECTIONS OF COLUMN

As Young's modulus of rebar is approximately 31 times as much as that of timber (Japanese Cedar) by bending, arrangement of rebars nearer the outer on cross-section will produce more increase of bending stiffness and strength. In the panel of connection between column and beam, development length of rebar of beam is required to

## 2 BACKGROUND

A study on rebar-mixed composite timber to improve bending stiffness and strength of timber beam was initialized by Granholm [3]. Also, after then, studies were and have been being conducted by using other materials beside rebar, however, most of the studies focused on only bending stiffness and strength of the composite beams under short-term or long-term loading. Connection between column and beam has nearly never been studied so as to use performance of the composite members, such as moment-resisting connection for rigid frame.

<sup>1</sup> Yuuto Shimoirisa, Department of Architecture,  
Kagoshima University, Japan, k2779317@kadai.jp

<sup>2</sup> Takahiro Iju, Takenaka Corp., Japan,  
iju.takahiro@takenaka.co.jp

<sup>3</sup> Takao Ohta, Kajima Corp., Japan, ohta-t@kajima.com

<sup>4</sup> Kazuya Mori, Takenaka Corp., Japan,  
mori.kazuya@takenaka.co.jp

<sup>5</sup> Shinichi Shioya, Department of Architecture,

Kagoshima University, Japan, k7347039@kadai.jp

be longer for transmission of axial force of the rebar between the composite beam and column.

On the other hand, in general, magnitude of axial force of columns for low-rise buildings is smaller than that for high-rise buildings. Therefore, the column for low-rise buildings is nearly never required comparative large cross-section area.

As a result of considering them, configurations for cross-section of column for low-rise buildings of two-way-frame may be chosen to be +, T, or L-shaped cross-section as shown in Figure 2, while rectangular portion (enveloped by red line in the figure) in the cross-section mainly resists lateral forces. Also, one-way frame may choose only rectangular cross-section according to planning of buildings. S.Shioya reported a loading experiment of one column specimen with + shaped cross-section for low-rise building [2] and two column specimens with square cross-section for middle rise building [4] . This paper reports an experiment of column specimens with rectangular, T, and a new +-shaped cross-sections.

#### 4 EXPERIMENTAL TEST FOR COLUMN WITH RECTANGULAR CROSS-SECTION

##### 4.1 SPECIMEN

Two columns with rectangular cross-section was selected with scale ratio of 2/3. Figure 3 illustrates the specimen. The specimen was modelled, considering connection between RC foundation and HGTSB column on ground floor of building. Area ratio of rebars (8-D16) to column’s gross-area (140mm x 400mm) was 2.8%. The column and RC foundation were connected by using the CFS at joint between rebar and jointing rebar at bottom of its column. The column bottom was connected to a reinforced concrete stub. After shaping the hybrid column, heat-resistant epoxy adhesive shown in Table 1 was filled in insertion hole on column bottom for joint rebar, and then the joint rebar ,8 pieces of D16 for this case, were inserted in the holes each to bond the built-in carbon fiber plastic sleeve (CFS) with the joint rebar. After the adhesive hardened, the column bottom and the RC stub were

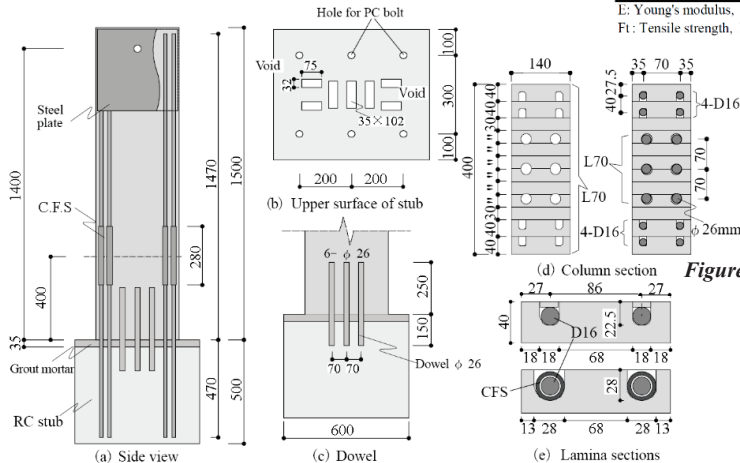


Figure 3: Specimen configuration and cross-section

connected by inserting its joint rebars into voids in the RC stub, for anchorage, and then filling non-shrinkage grout into the column bottom-stub gap and the voids of RC-stub simultaneously. Fresh concrete of nominal strength Fc42 was casted for concrete of the RC-stub. Nominal strength of the no-shrinkage grout is 61.3 N/mm<sup>2</sup> at 4 weeks. Glulam timber was prepared according to E65F255 in Japanese Agriculture Standard, and resorcinol-based resin adhesive was used for glulam timber. Table 1 lists Young's modulus and strengths of laminas of timber of which section size was 25×25mm<sup>2</sup>; the number was 10; loading was conducted as four-point bending. Strain was measured by foil strain gauges. Moisture content of lamina test pieces was 14.8%, and those density was 0.45g/cm<sup>3</sup>. Table 2 lists mechanical properties of rebar by testing. Table 3 lists mechanical properties in the catalogue of the epoxy adhesives used to bond the rebar.

##### 4.2 CARBON FIBER PLASTIC SLEEVE (CFS)

Figure 4 shows shape and dimensions of a CFS used, which is specified for joint rebar/deformed bar D16. Each rebar is inserted through holes at both ends of the CFS; the CFS is filled with epoxy adhesive shown in Table 3 to join both-side rebars in rigid. This joint was confirmed to produce rigid connection, as shown Figure 5. For more information on CFS, please refer to Reference 2 and 4.

##### 4.3 YIELD SECTION OF REBAR

As shown in Figure 6(a) in the next page, the joint rebar is devised to yield at the section between the RC stubs and the CFS, resulting in plastic elongation and contraction only over the section. The wood around the rebar is devised to be such that even if the rebar yields, the wood portion will not crack.

Table 1: Lamina properties

Grade	(Unit: N/mm <sup>2</sup> )			
	Bending test		Compressive test	
	E	F	E	F
L70	8663	68.4	8434	41.4

E: Young's modulus, F: strength

Table 3: Epoxy adhesive properties

(Unit: N/mm <sup>2</sup> )			
E	Fc	Ft	Fb
2200	76.4	43.4	64.9

E: Young's modulus, Fc: Compressive str  
Ft: Tensile strength, Fb: Bending strenth

Table 2: Rebar tensile properties

Rebar	(Unit: N/mm <sup>2</sup> )		
	E	$\sigma_y$	$\sigma_B$
D16	$1.96 \times 10^5$	371	558

L: Young's modulus,  $\sigma_y$ : Yielding strength  
 $\sigma_B$ : Braking strength

Table 4: CFS tensile properties

Specimen	(Unit: N/mm <sup>2</sup> )		
	E	$\sigma_y$	$\sigma_B$
D16	$1.94 \times 10^5$	363	557
CFS-1	$1.76 \times 10^5$	363	558
CFS-2	$2.11 \times 10^5$	352	557

E: Young's modulus,  $\sigma_y$ : Yielding strength  
 $\sigma_B$ : Braking strength

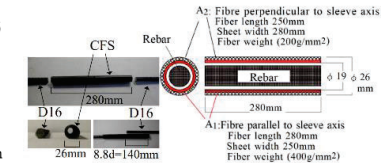


Figure 4: Carbon-fiber sleeve (CFS) and connection

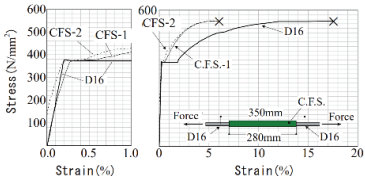


Figure 5: Tensile stress-strain of CFS

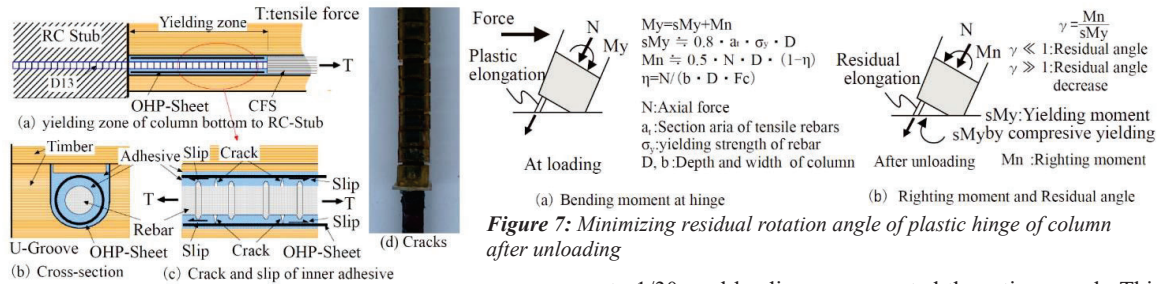


Figure 6: Yielding length for jointing rebar

#### 4.4 MECHANISM OF MINIMIZING RESIDUAL DEFORMATION OF COLUMN

As shown in Figure 7(a), yield bending moment/ $M_y$  of a column, which yields in bending by tensile rebar yielding, consists of the moment component/ $sM_y$  borne by the tensile rebar and the moment component/ $M_n$  borne by the axial force. The yielded rebar will generate plastic elongational deformation, resulting in plastic rotation angle in column bottom. After unloading, residual deformation occurs in the column due to its plastic rotation angle. In order to reduce the residual deformation, tensile-yielded rebar needs to yield in compression, and the reduction can be achieved by the moment/ $M_n$  by axial force.  $M_n$  is defined as restoring moment, and ratio of ' $M_n/sM_y$ ' is named as the restoring moment ratio/ $\gamma$ . When  $\gamma$  is larger than 1.0, the residual deformation of column decreases more. Moreover, when residual vibration after maximum response deformation of building during earthquake is taken into account, the plastic rotation angle can decrease even if ' $\gamma$ ' is smaller than 1.0.

#### 4.5 LOADING

Figure 8 shows set-up for loading. The vertical load/ $F_v$  was applied to column head; horizontal deformation at horizontal force height was gradually increased; the horizontal force was applied positively and negatively repeatedly, increasing the horizontal deformation.  $F_v$  divided by axial force capacity of column/ $N_u$  is defined as ' $\eta$ ' ( $=F_v/N_u$ ); axial force capacity/ $N_u$  is assumed to be product of compressive strength/ $F_c$  of glulam timber ( $F_c=20.6\text{N/mm}^2$ ) and cross-sectional area of the column ( $F_c \cdot b \cdot D$ ).  $b$  is column width and  $D$  is column depth. Figure 9 shows target displacement protocol for lateral loading. Target deformation angle/ $R_t$  was calculated by dividing the horizontal deformation by height  $h_F$  ( $=1400\text{ mm}$ ).

##### i) Specimen No.1(R16)

At first, axial force/ $F_v$  was maintained to be constant at an axial force ratio/ $\eta$  of 16%, and target deformation angle was gradually increased up to 1/50 rad. This is the first stage. After this, residual displacement was returned to zero and angle/ $R_t$  was returned to 1/200 and again  $R_t$  was gradually increased up to 1/50. This is the second stage. Additional residual vibration loading was applied at  $R_t$  indicated by symbol ' $\bullet$ ' in Figure 9 to investigate performance of minimizing residual deformation. The application rule for this residual vibration loading is described in the next section. This is the third stage. After this stage, in order to investigate the performance under unexpected Mega-earthquake,  $R_t$  was increased up

to 1/30. and loading was repeated three times each. This stage is the fourth stage. After this, the force was applied until fracture of column. This stage is the fifth stage.

##### ii) Specimens No.2 (R10) and No.2 (R30)

No.2 was one specimen, but No.2 (R10) was assumed to be characteristic during range where horizontal force was applied at  $\eta$  of 10% and No.2 (R30) was done to be that during range where the horizontal force was applied at  $\eta$  of 30%. With setting  $\eta$  being 10%, reversed repetitive loading was applied gradually increasing  $R_t$  from 1/400 to 1/50. This stage is the first stage of No. 2 (R10). After this, the vertical load/ $F_v$  was increased to  $\eta$  of 30%;  $R_t$  was returned to 1/400; lateral force was applied repeatedly with  $R_t$  gradually increasing up to 1/50. This is the first stage of No.2 (R30). The same process as the first stage was repeated three times, alternating  $\eta$  between 10% and 30%, as shown in Figure 9(b). These processes are the second, third, and fourth stages of No. 2 (R10) and No. 2 (R30), respectively. At the end of the fourth stage, No. 2 had experienced eight cycles of repetitive loading to 1/50. After this stage, with  $\eta$  setting 30%, repetitive loading was applied by increasing  $R_t$  to investigate the

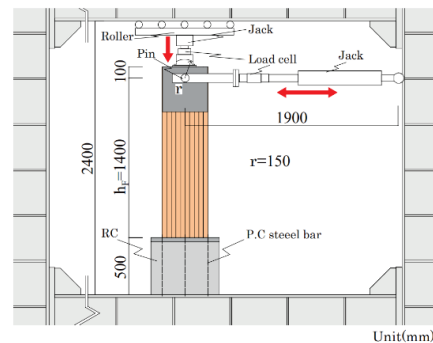


Figure 8: Set up for loading

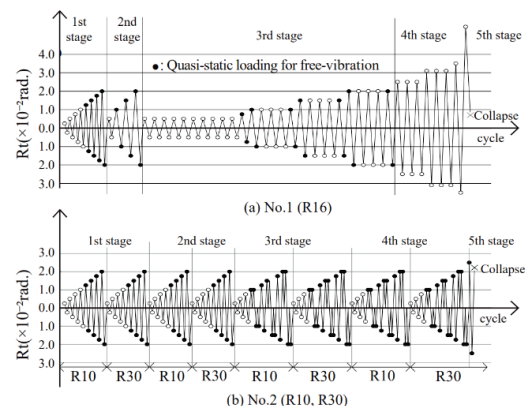


Figure 9: Target displacement protocol for lateral loading

performance during unexpected Mega-earthquake until fracture of column. This stage is the fifth stage.

#### 4.6 QUASI-STATIC LOADING FOR FREE-VIBRATION

In order to reveal that residual deformation be minimized after maximum response deformation during an earthquake, quasi-static loading was applied after it reached the target deformation angle/Rt by assuming damped free vibration. For more information of the loading force, please refer to previous reference [4]. Figure 10 schematically shows a hysteresis loop obtained by the loading. Final residual deformation ' $\delta_F$ ' was taken as the average of ' $\delta_2$ ' and ' $\delta_3$ '.

#### 4.7 MEASUREMENT METHOD

Figure 11 shows set-up for measurement of displacement and strain. Displacement transducer/Disp.1 and Disp.2 were used to measure horizontal deformation between the stub and horizontal force-applied point; Disp.3-Disp.6 were used to measure angle of rotation over hinge region of column bottom; Disp.7 and Disp.8 were used to measure shear slip deformation in the loading direction between column bottom and stub surface.

#### 4.8 EXPERIMENTAL RESULTS

##### 4.8.1 Failures and force-deformation relationship

Figure 12 shows final failures. Figure 13 and Figure 14 show horizontal force-deformation angle relationship.

i) No. 1 (R16)

Figure 13(a) shows relationship of the first stage. A tensile rebar yielded at  $R=+1/137$  rad. and bending capacity was almost determined. Figure 13(b) compares loop of the second stage with envelope of the first stage. In the first stage, initial stiffness was maintained up to  $+75.3$  kN at  $+1/137$ . In the second stage, the stiffness decreased at  $45.1$  kN and  $+1/235$ . This is due to the Bauschinger effect, as shown in Figure 3(d), where once steel yields, the proportional limit stress decreases in subsequent cyclic loading loops. Figure 13(c) compares envelope over the loops after the third stage with those of the second stage. The envelope of the second stage was almost the same as that of the third stage loops; Figure 13(e) and (f) and (g) show loops at typical target deformation angles. The first loop of the first stage is compared with last loop of the third stage; at  $R_1=1/100$ , the proportional limit is reduced as mentioned above; at  $R_1=1/50$ , loops of the first and third stages are almost identical. In the third stage, lateral force at  $R_t=1/400$  was applied 10 times, and thereafter, loading was repeated 5 times at each target up to  $1/50$ . When repetitive loading of the first and second stages were added, loading was applied at least seven times from  $1/400$  to  $1/50$ . Even with such many cyclic loadings, the loops after steel rebar yielded were hardly degraded. Figure 12(a) shows final failures. At the end of the third stage, no damage was observed in timber, and as shown in Figure 12, only thin cracks were observed on the top face of RC stub due to pull-out of joint rebar, and maximum width of cracks was less than  $0.3$  mm. The damage did not progress at all until the fourth cycle of  $1/30$ . Final fracture occurred at  $-1/140$  to negative direction after the loading was applied up to  $+1/18$ .

ii) No.2(R10) and No.2(R30)

Figure 14(a) and (b) show the first stage, in which tensile rebar of No.2(R10) yielded at  $+1/155$ . In No.2(R30), force at proportional limit also decreased due to the Bauschinger

effect because the joint rebar of column had already yielded at No.2(R10).

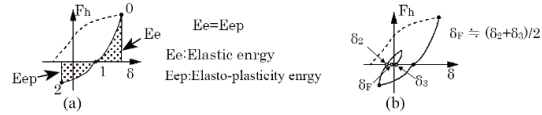


Figure 10: Quasi-static loading for free-vibration and determination final displacement

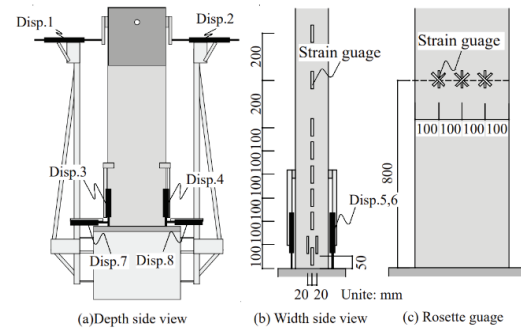


Figure 11: Set-up for measurement of displacement and strain

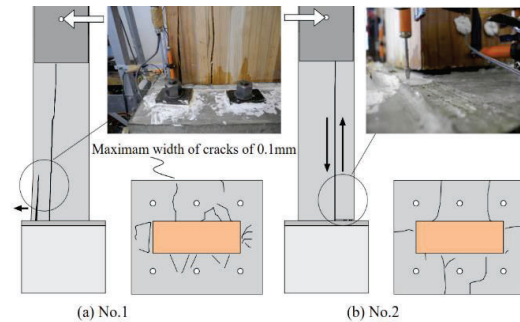


Figure 12: Observed failures until 5th stage

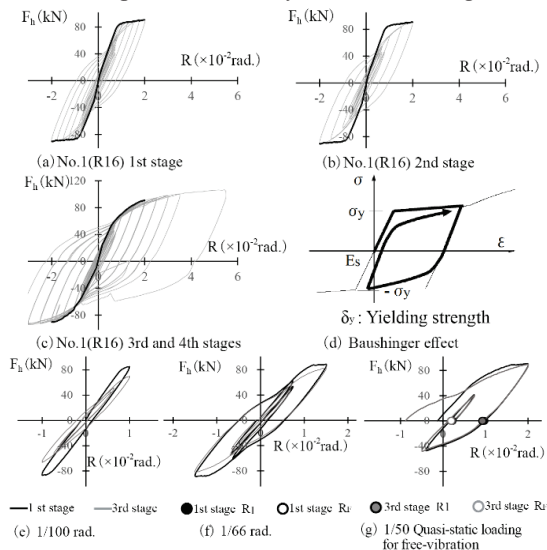


Figure 13: Lateral force-displacement angle relationship of NO.1



Figure 14(c) and (d) show the second stage. Envelope of the first stage is shown in comparison with that of the second stage: No.2 (R10) had a lower load at the proportional limit due to the Bauschinger effect; No.2 (R30) had also lower load at the proportional limit in the

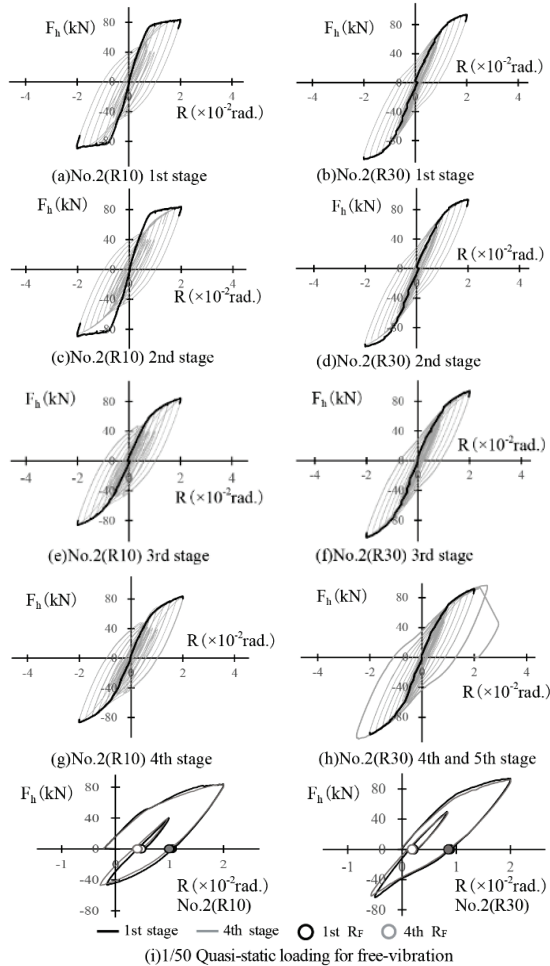


Figure 14: Lateral force-displacement angle relationship of NO.2

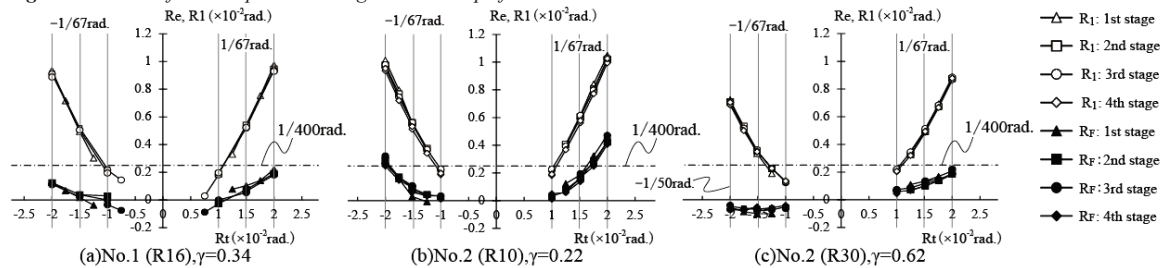


Figure 15: Relationship of residual displacement angle/ $R_f$ -target displacement angle/ $R_t$

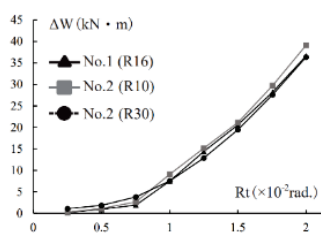


Figure 16: Dissipation energy

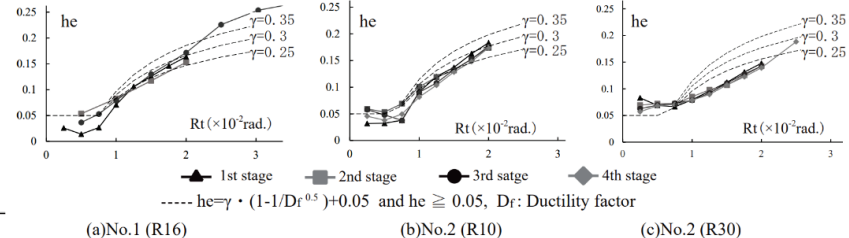


Figure 17: Equivalent viscous damping factor/ $h_e$

first stage; envelope of the first and second stages were almost the same in positive loading, and horizontal capacity of the second stage decreased slightly after 1/100 in negative loading.

Figure 14(e) and (f) show a comparison of the third-stage loop and the second-stage envelope; Figure 13(g) and (h) show a comparison of the fourth-stage loop and the third-stage envelope. Envelopes of the third stage almost encircle loops of the fourth stage, and no damage in column occurred after the fourth stage of No. 2 (R30). At the time, the column was subjected to eight cycles of incremental repetitive 1/400-1/50. After this, the fifth stage was applied to confirm final fracture with maintaining axial force ratio  $\eta$  of 30%. Figure 12(b) shows final failures. The column failed in shear with a vertically crack at the web at +1/45. From the results of No.1 and No.2 above, it is highly possible to realize a design in which the column connected to RC foundation are subjected to 8 cycles of incremental and repeated loading from 1/400 to 1/50, with axial force ratio  $\eta$  of 10-30%, with little damage and little degradation in loop after joint rebar yielded.

#### 4.8.2 Residual deformation suppression and restoring moment

Figure 13(g) and Figure 14(i) show examples of loops of residual vibration loading at  $R_t=1/50$ . Restoring moment ratio  $\gamma$  of each specimen was 0.34 for No.1 (R16), 0.22 for No.2 (R10), and 0.62 for No.2 (R30). Final residual deformation angle/ $R_f$  is indicated by symbol '○' according to the method of identifying residual deformation described in Section 4.6. The larger the restoring moment ratio/ $\gamma$  is, the smaller the final residual deformation angle is.

Figure 15 shows variation of residual deformation angle with the target deformation angle/ $R_t$  and compares each stage. It can be seen that the angle/ $R_f$  decreases from  $R_1$  due to the residual vibration loading, where  $R_f$  is deformation/ $R$  angle at  $\delta_F$  in Figure 10(b) and  $R_1$  is the deformation angle at  $\delta_1$ .

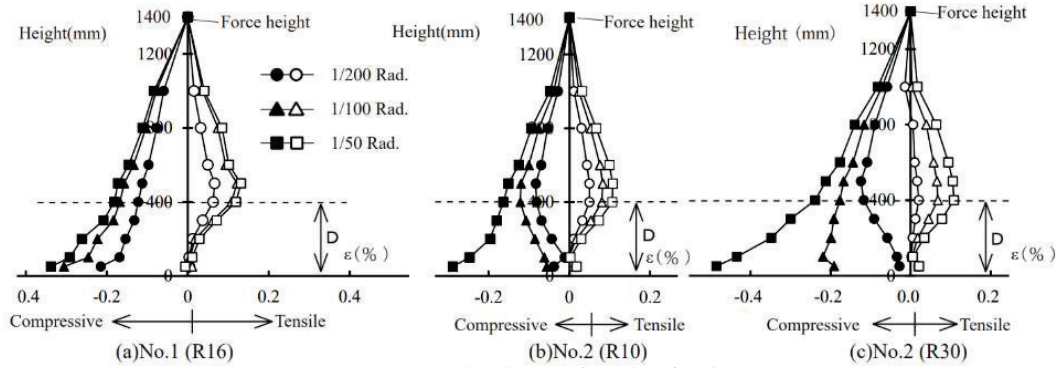


Figure 18: Strain distribution of wood surface by

Visually allowable limit angle of 1/400 for the residual deformation angle is shown in the figure as a horizontal, one dot chain line. This value is the upper limit of deformation angle at which column leaning cannot be visually recognized. If  $\gamma$  is greater than 0.34, the residual deformation angle was suppressed to 1/400 or less up to the range where target deformation angle was 1/50 or less.

#### 4.8.3 Dissipated energy and equivalent viscous damping constant

Figure 16 shows variation of the amount of dissipated energy at each target deformation angle loop. Since the dissipated energy is mainly plastic energy by yielding of joint rebar in column, cycles with the same target deformation angle had similar amount in irrespectively of the magnitude of axial force.

Figure 17 shows variation in the equivalent viscous damping constant/ $h_e$  of each loop.  $h_e$  is smaller for larger values of axial force ratio/ $\eta$ . As  $h_e$  is calculated by dividing the amount of dissipation energy of loop by the target deformation and its capacity, larger axial force ratio decreases more the value of  $h_e$ . It is necessary to consider the effect of axial force for  $h_e$ .

#### 4.8.4 Distribution of strain in column by bending

Figure 18 shows distribution of vertical strain of wood surface by bending. On the compressive surface, the strain distribution increased at the column bottom. On the tensile surface, distribution of strain increases downward from force applied point of column head and decreased to zero from a height of 400 mm to column base. The range is demonstrated not to adhere to the assumption of the plane section used for calculation of bending capacity and stiffness.

#### 4.8.5 Estimation for stiffness and bending capacity

Elastic stiffness was calculated for three cases shown in Figure 19. The column bottom was assumed to be fixed-ended; Cal.1 in Figure 19(a) was calculated using the cross-sectional secondary moment/ $E_w I_e$  including the rebar. Cal.2 in Figure 19(b) was calculated using the flexural stiffness  $E_w I_w$  of Glulam timber column by ignoring rebar. Cal.3 in Figure 19(c) was calculated by dividing the hinge of column bottom into two half section, with the bending stiffness of the half section on the base side as bending stiffness/ $E_s I_s$  resisted by only joint rebar and bending stiffness of the upper half section as average of bending stiffness / $E_w I_e$  of the composite column and  $E_s I_s$ . The reduction of tensile strain of wood near the

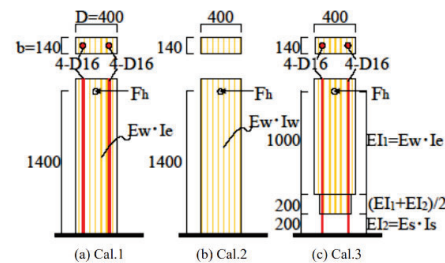


Figure 19: Assumed bending stiffness for calculations

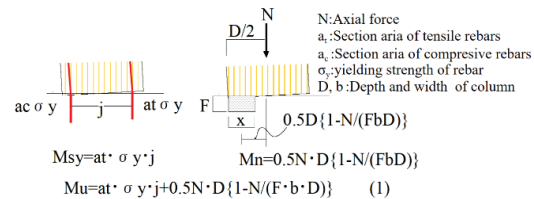


Figure 20: Stress assumed for ultimate bending moment

column bottom in Figure 18 was taken into account. Length of the hinge was assumed to be 400 mm of column depth. This is Cal.3. Shear deformation was considered as resisted by the cross-section of timber, with a shape factor of 1.2 and ignoring the rebar. Shear modulus of elasticity of wood was assumed to be 800 N/mm<sup>2</sup> referring to the shear strain in Figure 11(c). Young's modulus for timber and rebar were based on material test. Figure 21(a) shows loops of horizontal load -deformation angle relationship for No. 1 (R16); the calculated elastic stiffnesses are indicated as straight lines of thick, thin and one dot chain line. The experimental elastic stiffness is between Cal.1 and Cal.2 and close to the elastic stiffness of Cal.3. Figure 21(b) compares those of calculation with the envelope up to joint rebar yielding. On the positive loading, the stiffness by Cal.3 estimates experimental stiffness, while, on the negative loading, the experimental stiffness is somewhat larger. The load-deformation angle relationship calculated by replacing wood of specimen with concrete of compressive strength/ $F_c$  (30N/mm<sup>2</sup>) is shown in the figure by one dot chain line. The column base was assumed to be fixed ends, taking into account rebar for the bending stiffness of column. The stiffness of RC column is greater until flexural crack occurs, after which The stiffness decreases and approaches that of the specimen. It can be confirmed that the stiffness of the composite columns is close to that of RC column. The capacity was determined by dividing the bending capacity moment/ $M_u$

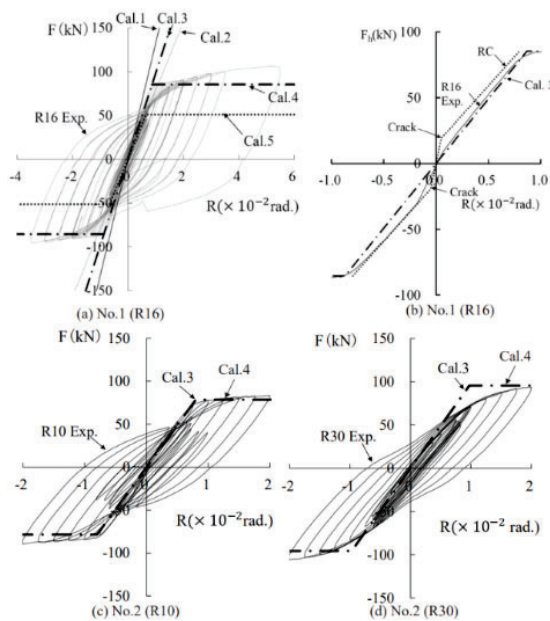


Figure 21: Skeleton curves of experiment loop and calculation

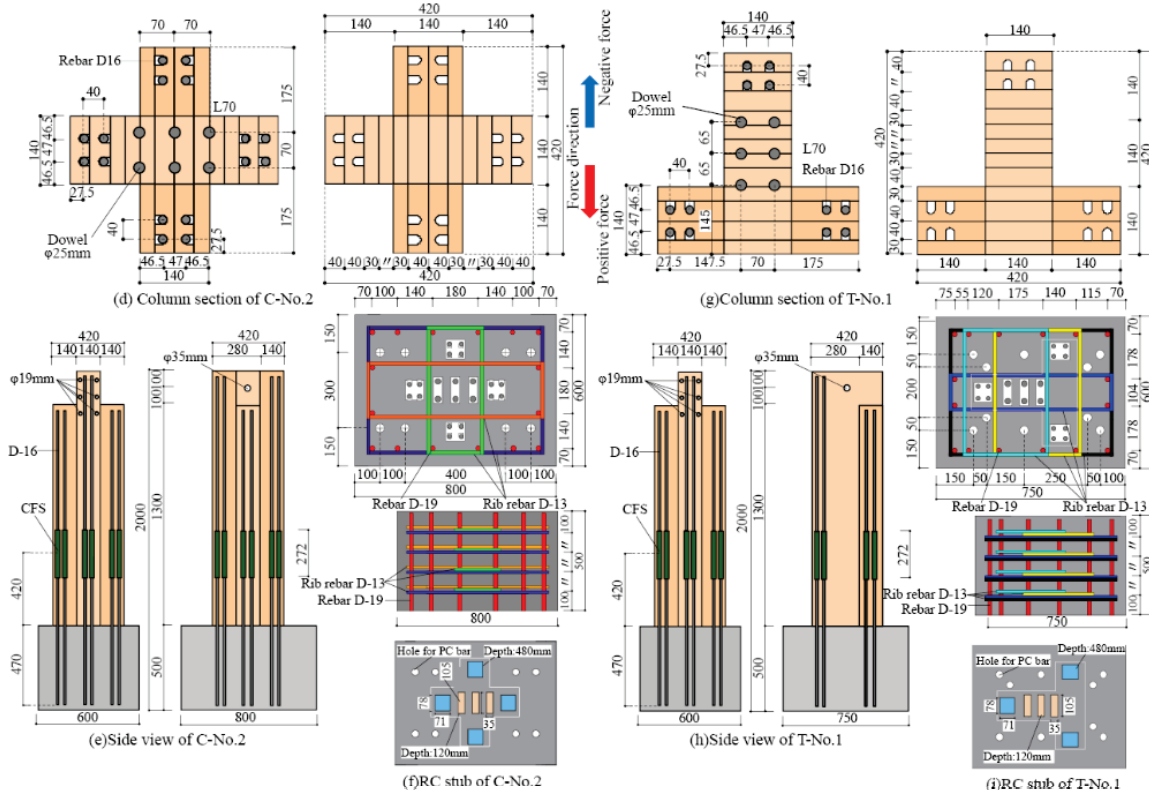
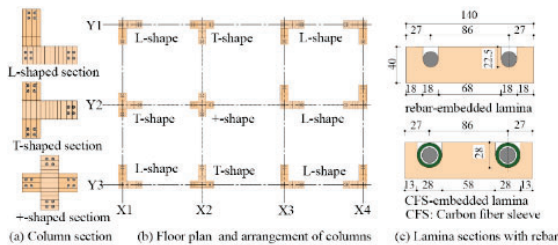


Figure 22: Configuration, cross-section, and details of specimens

by the horizontal loading height ( $h_F=1400$  mm) where the joint rebar of column bottom yields, as shown in Figure 20. Sum of bending moment/ $M_{sy}$ , which can be resisted by joint rebar in yielding, and bending moment/ $M_n$ , which can be resisted by axial force/ $N$  and compressive zone of wood. This capacity is Cal.4. Yield strength of rebar was taken as a material test value and compressive strength/ $F_c$  of timber was taken as  $22.5$  N/mm<sup>2</sup>, which is a standard value for timber. It can be seen in Figure 21(a) that the calculated capacity almost estimates the capacity at which the rebar yields.

In Figure 21(a), bending capacity of Glulam timber column in Figure 19(b) is shown by horizontal dotted line, where the timber is assumed to reach its bending capacity at column bottom. This is Cal.5. The yield capacity of the specimen is 167% of Cal.5, confirming that connection capacity for the composite column base is extremely high. Figure 21(c) and 21(d) show No. 2; in Figure 21(d), R30 experienced the loading up to 1/50 at No.2(R10) and then started the loading, so that the stiffness of column was reduced before yielding due to the Bauschinger effect and the experimental stiffness was smaller than the calculated relationship. Excluding this, it can be found that skeleton curve by Cal. 3 and Cal. 4 can estimate roughly skeleton curve of experimental force-deformation angle loops.

## 5 LOADING TEST FOR COLUMN WITH + AND T-SHAPED CROSS-SECTION

As described in Chapter 3, in low-rise buildings, there are three possible shapes of column cross-sections in terms of



architectural plan, as shown in Figure 22(a); L-shaped section column alone, as seen between the X3-X4 axes in Figure 22(b), can constitute a two-way rigid frame.

The L-section column is desirable because of the fitting of column and wall and because of the efficiency of the use of room and corridor.

The L-section column also have the advantage of having only one secondary bonding surface in production.

However, L- section column is difficult to apply in loading test due to eccentricity. If the floor slab is provided for the entire building, effect of the eccentricity in the column is negligible small and therefore, the mechanical performance of the L-shaped column in building will approach that of T-shaped section column.

In this study, it was determined to investigate performance of T-shaped section column specimen.

A horizontal loading test have already been carried out on +-shaped section columns subjected to strong-axis bending of Glulam timber to reveal their elasto-plastic characteristics [2]. This horizontal loading test were carried out on a +-shaped section column subjected to weak-axis bending and a T-shaped section column to investigate the elastic-plastic properties, and the method for estimating the skeleton curve of horizontal load-deformation angle relationship was discussedd.

### 5.1 SPECIMEN

Figure 22(d)-(i) show cross-sections, shapes, and dimensions of specimens. The number of specimens was two: one with a + shaped cross-section (C-No.2) and the other with a T-shaped cross-section (T-No.1). The height

Table 5: Mechanical properties of lamina and rebar

(a)Lamina (Unit: N/mm <sup>2</sup> )				(b)Rebar (Unit: N/mm <sup>2</sup> )				
Grade	Compression		Bending	Rebar	a <sub>0</sub> in mm <sup>2</sup>	E	σ <sub>y</sub>	σ <sub>b</sub>
	E <sub>c</sub>	F <sub>c</sub>	E <sub>b</sub>	F <sub>b</sub>				
L70	8835	34.1	9639	63.6	D16	198.6	1.97x10 <sup>5</sup>	389 571

F<sub>c</sub>,F<sub>b</sub>: Strength  
 E<sub>c</sub>,E<sub>b</sub>: Young's modulus  
 a<sub>0</sub>: Nominal cross-sectional area of rebar  
 F: Young's modulus, σ<sub>y</sub>: Yielding strength  
 σ<sub>b</sub>: Breaking strength

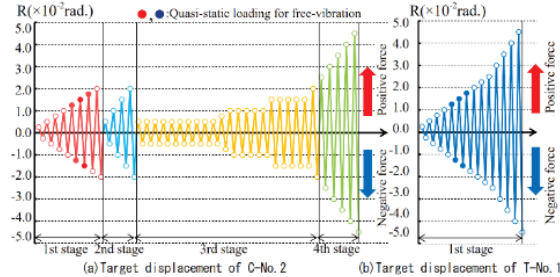


Figure 23: Target displacement protocol for lateral loading

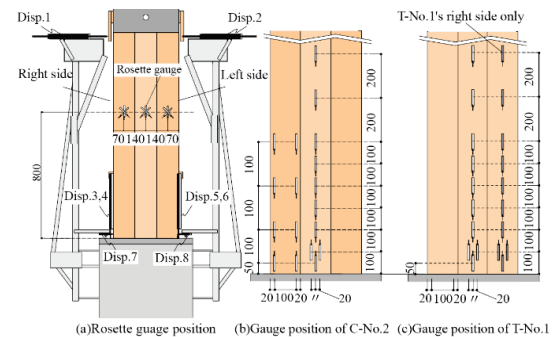


Figure 24: Set-up for measurement of displacement and strain

of force point was 1400 mm. Scale of specimen was approximately 2/3 of actual dimensions. The columns were manufactured by first gluing together a rectangular section of 140 x 420 mm (hereafter referred to as the main section) and a square section of 140 x 140 mm (hereafter referred to as the orthogonal 'Part A'), and then gluing these sections together into a +-shaped cross-section and a T-shape section. The +- shaped section column had a total rebar area ratio  $p_g$  of 3.24% and a tensile rebar area ratio  $p_t$  of 1.62%; the T-section column had a total rebar area ratio  $p_g$  of 2.43% and a tensile rebar area ratio  $p_t$  of 1.62%. The connection of RC stub and column bottom and the yield length of rebar was the same as in Section 4.3. Glulam timber was JAS cedar laminated timber of the same grade E65F255 (with finger joints) and adhesive for gluing was resorcinol-based resin. Table 5(a) lists mechanical properties of lamina by testpieces. Table 5(b) lists mechanical properties of rebar by testpieces.

### 5.2 LOADING AND MEASUREMENT

Method and system for loading were the same as in Figure 8. The axial force on column was chosen to be 194 kN as the axial force ratio  $\eta$  of 10%, while axial force on the T-shaped section column was chosen to be 121 kN as the axial force ratio  $\eta$  of 6%. The axial capacity  $N_u$  is the product of the compressive strength  $F_{wc}$  (20.6 N/mm<sup>2</sup>) of standard strength of Glulam timber and the gross cross-sectional area of timber in the column. The deformation angle is the same as Section 4.5.

### 5.3 EXPERIMENTAL RESULTS

Figure 25 shows final failures and Figure 26 shows the horizontal load-deformation angle relationship of column in the first stage.

i) +-shaped section column (C-No.2)

Under positive loading, rebar in tensile side yielded in tension at +1/118 at +95.0 kN ( $Y_{t1}$ ), while rebar in compressive side also yielded in compression ( $Y_{c1}$ ). After this, the second-tier rebar in the tensile side yielded in tension at +1/100 rad., +99.4 kN ( $Y_{t2}$ ) and the second-tier rebar in the compressive side yielded in compression at +1/78, +105.0 kN ( $Y_{c2}$ ). These points are shown in Figure 26. After the rebars yield, horizontal stiffness decreased and the load increased at a constant stiffness, i.e., the secondary stiffness. This is seemed to be due to the rebar in Part A still being in elastic and the stiffness of wood in compression. At the peak of the cycle (+121.4 kN, +R=1/57) when the target deformation angle/Rt was +1/57., strain of rebar in the tensile side of Part A was 1743  $\mu$  and it had not yielded yet. At R=-1/59, -125.5 kN on the negative loading, as shown in Figure 25(a), a vertical crack occurred in the Part A near the border with the main section, and then load dropped rapidly. This was the time of maximum load. At this time, strain of the rebar in the main section was 1804 $\mu$  and it had not yielded yet. From these results, it can be concluded that the specimen failed in shear before the column bottom reached ultimate bending capacity. It is explained that the rebar in the orthogonal sections increased bending capacity and increased shear force of column, and, as a result, shear failure occurred. After this, the column split in two by the



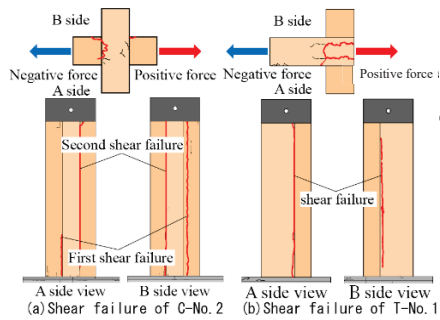


Figure 25: Failures until final

vertical crack and resisted horizontally and exhibited horizontal capacity and provided a stable loop up to  $\pm 1/50$  rad. After this, residual deformation was returned to 0.0 mm, and the second stage of loading was applied repeatedly by gradually increasing the target deformation angle from  $\pm 1/200$  to  $\pm 1/50$ .

Figure 27(a) compares loops of the second stage (solid black line) with the final  $\pm 1/50$  loop of the first stage (red dotted line). The black loops are enveloped by the red dashed loop, and after the vertical cracking, a stable loop was exhibited by the segmented elements. Figure 27(b) and (c) show loop of the third stage and the loop of the fourth stage at  $R_i = \pm 1/50$ . The red dashed loop is the same as those in Figure 27(a).

In Figure 27(b), the loop of  $R_i = 1/50$  exhibited almost no deterioration, and in Figure 27(c), it exhibited +114.5 kN up to  $R_i = +1/33$  on positive loading. However, immediately after that, at +100.6 kN during unloading, new vertical cracks occurred as shown in Figure 25(a). After this, the stiffness and capacity decreased in both negative and positive loading, and the capacity was +68.2 kN in the positive loading and -76.3 kN in negative loading. The column resisted as three separated elements and exhibited stable loops up to  $R = +1/22$  such that they could resist the vertical load until the final deformation. Because of the presence of rebars within the divided elements, they could resist to axial forces and a constant horizontal force, even when split by shear failure.

(b) T-shaped section column

On the positive direction, the first outer rebar in tensile side yielded in tension at  $R = +1/123$  at +97.8 kN ' $Y_{t1}$ ' and the second rebar in tensile side yielded in tension at  $R = +1/113$  at 98.2 kN ' $Y_{t2}$ '. At this, it can be judged that bending capacity had almost been reached. After this, the load increased with a constant and gradual stiffness, which might be caused by the elastic resistance of the rebar near the tensile side among the two-tier rebar in the flange of the T-section.

On the negative direction, the first rebar in the tensile side yielded in tension at  $R = -1/117$  ' $Y_{t1}$ ', and the second-tier rebar yielded in tension at  $R_t = -1/65$ , -134.7 kN, slightly exceeding yielding strain/ ' $Y_{t2}$ '. Compressive yielding of rebar in the compression could not be judged from strain gauge values because the rebar had already yielded on the positive direction. Immediately after this, as shown in Figure 25(b), vertical cracks occurred so that the

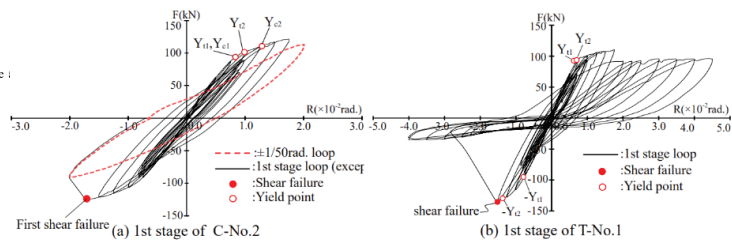


Figure 26: Lateral force-displacement angle relationship of 1st stage

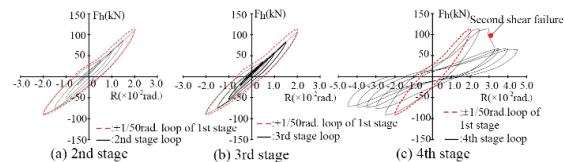


Figure 27: Lateral force-displacement angle relationship of C-No.2

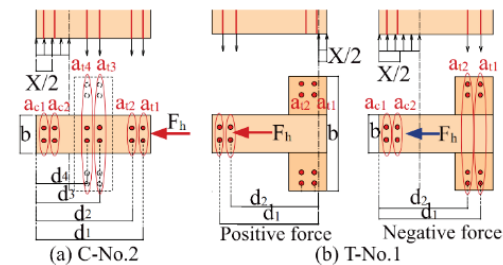


Figure 28: A model for C-No.2 and T-No.1 at bending capacity

orthogonal section (Part A) and the main section were separated, resulting in a sudden drop in load.

It can be judged that the specimen, on the negative loading, failed in shear just before reaching the bending capacity. After this, the two separated elements resisted as a column, respectively, and capacity on the positive loading was +94.8 kN. The negative load capacity was -34.5 kN.

Even with T-shaped cross-section, care should be taken in design of the column because the bending capacity increases in the direction of loading in which the orthogonal columns are in tension, resulting in shear failure due to the increased shear force.

### 5.3.1 Elastic stiffness

As well as the calculation in Section 4.8.5, a hinge section in the column bottom was assumed to be column depth of 420 mm.

### 5.3.2 Yield bending capacity

Equation (1) in Figure 20 can be modified to apply to + and T-shaped cross-sections as follows. Figure 28 shows symbols for assumed cross-sections and dimensions.

$$M_r = \sum \alpha_i \cdot a_{ti} \cdot \sigma_y \cdot j_i \quad (2)$$

$$M_n = 0.5 \cdot N \cdot D \cdot (1 - X) \quad (3)$$

$$M_u = M_r + M_n \quad (4)$$

where,  $a_{ti}$ ,  $a_{ci}$ : Gross cross-sectional area of rebar in each tier as tensile rebar or compressive rebar,  $\sigma_y$ : yield strength of rebar,  $\alpha_i$ : Adjustment factor for stress at bending capacity,  $j_i$ : Distance from the centroid of the combined compressive forces to each rebar tier,  $j_i = d_i - X/2$ ,  $X$ : Depth of the bending and compressive zone

$$X = (N + \sum \alpha_i \cdot a_{ti} \cdot \sigma_y - \sum \alpha_i \cdot a_{ci} \cdot \sigma_y) / (F_{wc} \cdot b) \quad (5)$$

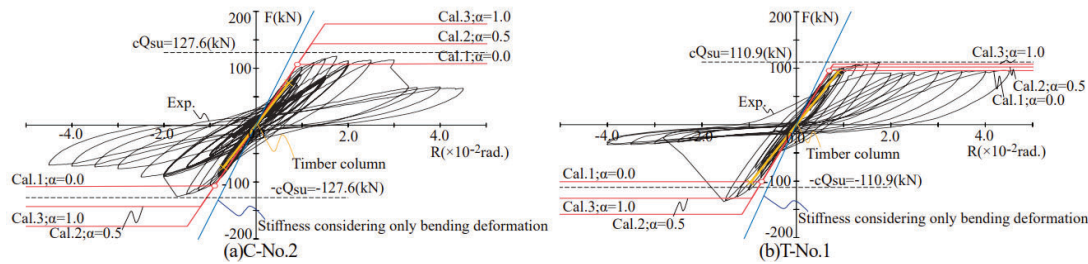


Figure 29: Comparison of calculation to experiment of skeleton curve of lateral force-displacement angle

### 5.3.3 Calculation and Experimental Result

Figure 29 shows a comparison of the calculated result of the skeleton curve and the experimental loops. Initial stiffness was calculated separately for bending and shear deformation. Material test values were used for wood and rebar.

#### (a) Elastic stiffness

The bending stiffness, assuming the plane cross-section, was calculated for total cross-section area, taking rebar into account. The shear modulus of wood was assumed to be 812 N/mm<sup>2</sup> and the shape factor of shear deformation to be 1.68. The shear resistance area is the horizontal cross-section area of the main cross-section of the wood, the column bottom and in the section from the column head down to column depth. The intermediate section between those were assumed to be the cross-section area of the full cross-section, including the orthotropic sections.

Initial stiffness with only the bending deformation component is shown by blue solid line. The relationship with red solid line shows that added shear deformation. By considering shear deformation, the initial stiffness of both specimens has been accurately estimated by the model shown in Figure 19.

#### (b) Yielding capacity

+shaped section columns were assumed to be tension-yielded or compression-yielded, with four two-tier rebar groups on either side of the main section, concentrated at the centroid of each group. The  $\alpha_i$  in Equation (5) for rebar is assumed to be values at range of 0.0-1.0; the eight rebars in the orthogonal section were also concentrated in the center of the column cross-section. The calculated capacity with  $\alpha_i = 0.0$  is indicated by symbol '○' as yielding capacity. Shear force was calculated by dividing the yield moment by the height from the loading point to base. Both positive and negative capacities were approximately estimated. After yielding, the column attempted to reach Cal. 3 capacity, i.e.  $\alpha_i = 1.0$ , but it was seemed its shear force had reached the shear capacity and then shear failure has occurred.

The number of rebars resisting in tension in T-shaped section column depends on direction of loading. For positive loading, the two-tier rebar in tensile side were assumed to yield and the  $\alpha_i$  of the third rebar in the flange at the orthogonal section was assumed to 0.0, 0.5 and 1.0, where compressive reinforcement bars were neglected. On the negative loading, four rebars in the first-second tiers from the compressive side in the main section were assumed to yield in compression, the first-tier rebar from the tensile side was assumed to yield and  $\alpha_i$  was set to 0.0, 0.5 and 1.0 to the second-tier rebar. Yield capacity ○ with  $\alpha_i$  being to 0.0 approximately estimates capacity at the positive and negative proportional limits of the

experiment. The column width/b was assumed to be 420 mm for the positive loading and 140 mm for the negative loading. In the future, we are going to investigate a method for estimating the shear capacity.

## 6 CONCLUSION

Horizontal loading tests were conducted on rectangular, +, and T-shaped cross-sectional columns of which bottoms were planned to yield by bending, assuming the first floor of low-rise building consisting of rigid joined frame using HGTSB, and the elasto-plastic behavior of the column was clarified. The results are summarized below.

- 1) The horizontal stiffness and the bending capacity of the column was higher than those of ordinary glulam timber column with its same cross-section assuming that the column bottoms were fixed-end.
- 2) When the column axial force ratio was less than 0.25, they were hardly damaged even after subjected many times, of which one is cyclic loading from 1/400 to 1/50. After joint rebars of the column bottom yielded, its loops were shaped to exhibit abundant energy dissipation. The only degrading property was the reduction in bending moment of the proportional limit, due to the Bauschinger effect that occurs after the rebar yield.

## ACKNOWLEDGEMENT

This project was funded as Grants-in-Aid for Scientific Research-B by Japan Society for the Promotion of Science.

## REFERENCES

- [1] S. Shioya: Hybrid timber-steel bar glulam and its building system. JTCCM JOURNAL, Vol.52, 2016.
- [2] S. Shioya, et al.: An innovative hybrid timber structure in Japan: performance of column and beam. World Conference on Timber Engineering, 2016.
- [3] Granholm, H.: Armerat Tra (Reinforced timber), Chalmers Tekniska Hogskolas Handlingar. No.154, 68-76, Gothenburg, Sweden, 1954.
- [4] M. Mukai, et al.: Horizontal - loading test of steel bar - timber composite column for mid-rise building. World Conference on Timber Engineering, 2021.
- [5] N. Fukutomi, S. Shioya, et al.: Design Method to Estimate Stiffness and Strength of Hybrid Timber-Steel Beams. World Conference on Timber Engineering, 2018.